Received: 27 September 2023 | Revised: 13 December 2023 | Accepted: 19 December 2023

DOI: 10.1002/dad2.12526

Alzheimer's & Dementia
Diagnosis, Assessment & Disease Monitoring

RESEARCH ARTICLE

Personalized modeling of Alzheimer's disease progression estimates neurodegeneration severity from EEG recordings

Lorenzo Gaetano Amato[1,2] | **Alberto Arturo Vergani**[1,2] | **Michael Lassi**[1,2] | **Carlo Fabbiani**[3,4] | **Salvatore Mazzeo**[3,4] | **Rachele Burali**[3] | **Benedetta Nacmias**[3,4] | **Sandro Sorbi**[3,4] | **Riccardo Mannella**[5] | **Antonello Grippo**[3] | **Valentina Bessi**[4] | **Alberto Mazzoni**[1,2]

[1]The BioRobotics Institute, Sant'Anna School of Advanced Studies, Pisa, Italy

[2]Department of Excellence in Robotics and AI, Sant'Anna School of Advanced Studies, Pisa, Italy

[3]IRCSS Fondazione Don Carlo Gnocchi, Florence, Italy

[4]Department of Neuroscience, Psychology, Drug Research and Child Health, Careggi University Hospital, Florence, Italy

[5]Università di Pisa, Dipartimento di Fisica, Pisa, Italy

Correspondence
Lorenzo Gaetano Amato and Alberto Mazzoni, The BioRobotics Institute, Sant'Anna School of Advanced Studies, 56127 Pisa, Italy.
Email: LorenzoGaetano.Amato@santannapisa.it and alberto.mazzoni@santannapisa.it

ClinicalTrials.gov Identifier: NCT05569083

Funding information
Tuscany Region—Predicting the Evolution of SubjectIvE Cognitive Decline to Alzheimer's Disease With machine learning, Grant/Award Number: CUP.D18D20001300002; Ministry of University and Research (MUR), National Recovery and Resilience Plan (NRRP), project THE, Grant/Award Number: IECS00000017; Ministry of University and Research (MUR), National Recovery and Resilience Plan (NRRP), project MNESYS, Grant/Award Number: PE0000006

Abstract

INTRODUCTION: Early identification of Alzheimer's disease (AD) is necessary for a timely onset of therapeutic care. However, cortical structural alterations associated with AD are difficult to discern.

METHODS: We developed a cortical model of AD-related neurodegeneration accounting for slowing of local dynamics and global connectivity degradation. In a monocentric study we collected electroencephalography (EEG) recordings at rest from participants in healthy (HC, $n = 17$), subjective cognitive decline (SCD, $n = 58$), and mild cognitive impairment (MCI, $n = 44$) conditions. For each patient, we estimated neurodegeneration model parameters based on individual EEG recordings.

RESULTS: Our model outperformed standard EEG analysis not only in discriminating between HC and MCI conditions (F1 score 0.95 vs 0.75) but also in identifying SCD patients with biological hallmarks of AD in the cerebrospinal fluid (recall 0.87 vs 0.50).

DISCUSSION: Personalized models could (1) support classification of MCI, (2) assess the presence of AD pathology, and (3) estimate the risk of cognitive decline progression, based only on economical and non-invasive EEG recordings.

KEYWORDS
Alzheimer's disease, Computational models, Computational neuroscience, EEG, Novel Biomarkers

Highlights

- Personalized cortical model estimating structural alterations from EEG recordings.
- Discrimination of Mild Cognitive Impairment (MCI) and Healthy (HC) subjects (95%)
- Prediction of biological markers of Alzheimer's in Subjective Decline (SCD) Subjects (87%)
- Transition correctly predicted for 3/3 subjects that converted from SCD to MCI after 1y

1 | BACKGROUND

Alzheimer's disease (AD) is the major form of dementia, with more than 10 million people worldwide suffering from it.[1] This number is expected to rise to 50 million in 2050,[2] and several steps forward in AD research are needed to face this challenge. The disease develops a distinct symptomatology only years or decades after its initial stages, with a progressive decline in memory and other functions. Early diagnosis of AD is therefore a key goal in addressing the progression of the disorder. In the past years, growing attention has been paid to the prodromal and preclinical phases of AD. A prodromal phase is the subjective cognitive decline (SCD) condition,[3] in which the patient reports a self-concerned experience of reduced cognitive function, while maintaining normal scores on standardized cognitive tests. In the mild cognitive impairment (MCI) condition,[4] the effect on the patient's cognition is detectable with standardized tests (see[4] and Methods), but there are no direct effects on everyday life. These conditions, although linked to an increase in probability of transition to overt AD,[3] are a weak proxy of the disease presence, with many people suffering from them without ever transitioning to overt AD. SCD patients are a very diverse group in both evolution and manifestation of the disease, with little prediction power about progression to AD given by the SCD diagnosis alone.[3] Nowadays, some diagnostic power about AD progression has been achieved capturing the structural and functional alterations due to the disease with magnetic resonance imaging (MRI) and positron emission tomography (PET) scans,[5,6] or cerebrospinal fluid (CSF) profiles.[7] However, these procedures are either expensive for the medical facility or discomforting and/or painful for the patient.[8] Evaluation of prodromal and preclinical phases of AD through electroencephalography (EEG), which is an affordable and non-invasive procedure, is currently limited to quantifying EEG features known to be biomarkers of the disease,[9,10] such as spectral features and functional connectivity (FC) between brain regions.[11,12] Despite some interesting results,[13] EEG biomarkers fall far behind those obtained from imaging techniques such as MRI and PET scans.[14]

The approach that we propose to overcome this issue is that of the personalized brain models.[15] We present a computational framework in which a network model simulating cortical activity evolves from a healthy condition (HC) toward AD, with progressively degenerating local synaptic and global connectivity parameters (respectively *lp* and *cp*). In this way, knowing the specific EEG features of a given patient we can estimate the values of local and global degeneration (from *lp* and *cp* parameters) and hence evaluate the stage of the patient in the evolution toward AD. Briefly, we proceeded as follows (Figure 1). First, we extracted standard biomarkers from experimental EEG recordings (spectral content and FC, Figure 1 top row) of patients (grouped as SCD, MCI, and HC), and we assessed the ability of these features to discriminate between the patient groups (Figure 1, top right). Then we developed an AD progression model starting from The Virtual Brain (TVB) platform[16–19] framework. We developed a network model in which AD progression is described by two parameters depicting local micro-circuital and global macro-scale structural alterations of the network caused by AD[20] (Figure 1, bottom left). The model was validated by comparing the simulated signal features with population data in the three groups. Patient-specific values of local and global degeneration (network features) were then estimated from the individual values of the experimental EEG features (Figure 1, bottom middle). We then assessed the diagnostic efficacy of these network features in discriminating between patient groups (Figure 1, bottom right) and we compared it with the performance of the EEG features. Finally, we compared the efficacy of both EEG and network features in predicting the presence of AD pathology (previously assessed by CSF extraction[7]) from EEG recordings. We also validated these predictions with the outcome of the 1 year follow-up for SCD patients.

RESEARCH IN CONTEXT

1. **Systematic review**: The authors reviewed the literature using standard sources (eg, Scopus) with relevant keywords, alongside meeting abstracts and presentations. All relevant works (particularly those focusing on early diagnosis) are cited.
2. **Interpretation**: We present a novel model of Alzheimer's-related neurodegeneration enabling mild cognitive impairment classification from EEG and shedding light on the relations between structural alterations and functional anomalies observed in the EEG of pre-demented subjects. Moreover, we predicted with unprecedented precision the presence of biological culprits of the disease before symptoms onset, all from a simple, non-invasive scans.
3. **Future directions**: This study proposes a novel diagnostic pipeline for the early detection of Alzheimer's disease. Further improvements and validation of our approach could include (1) validation based on comparison with structural data; (2) longitudinal study of longer duration for assessing the prediction of possible clinical outcomes; and (3) translational use of the model for simulating therapeutic approaches.

2 | METHODS

2.1 | Participants: Recruiting and diagnosis

Patients included in this study were recruited as part of a clinical neuropsychological-genetic inquiry on pre-AD conditions such as SCD and MCI (ClinicalTrial.gov identifier: NCT05569083). All patients self-referred to the Centre for Alzheimer's disease and Adult Cognitive Disorders of the Careggi Hospital in Florence, Italy. Relevant demographic information on enrolled participants can be found in Table S1. Inclusion and exclusion criteria follow standard clinical guidelines and are described in detail in the Supplemental Materials. All patients

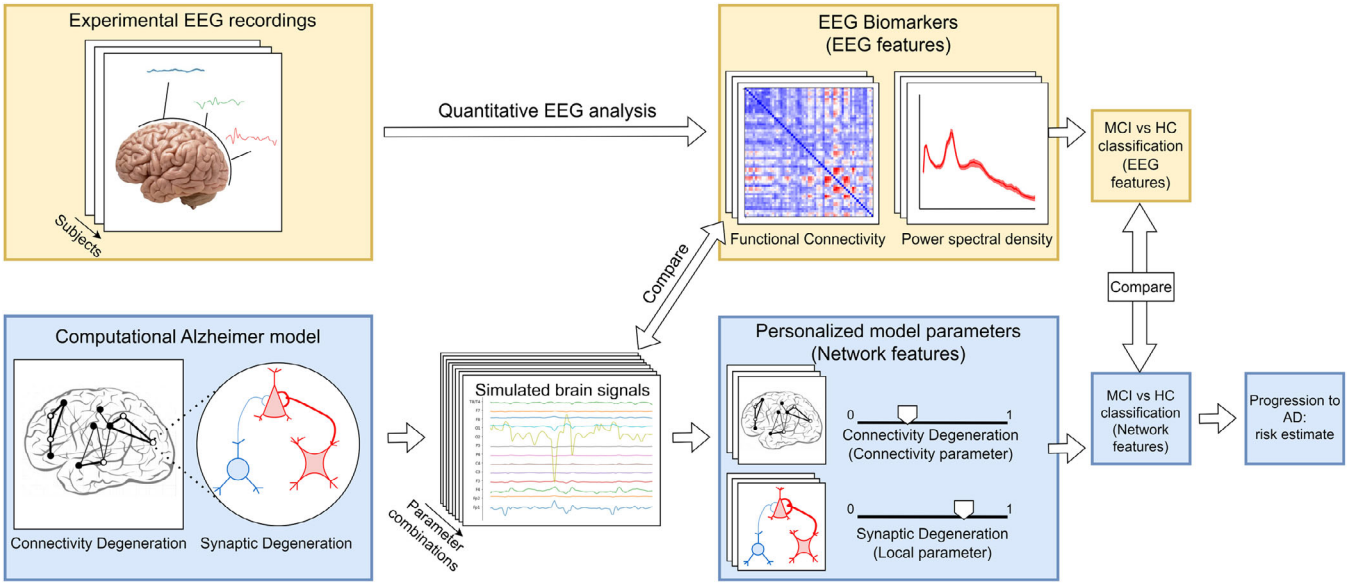

FIGURE 1 Workflow summary. Top row, left to right: EEG data are acquired from HC subjects and patients with SCD and MCI. The most group-informative EEG features based on spectral and FC analysis are extracted and then used to discriminate between HC and MCI. Finally, the same algorithm partitions patients with SCD according to their probability of progressing to AD, deduced from biological hallmarks of the disease. Bottom row, left to right: Development of a network model of neurodegeneration in TVB frame based on two parameters, a local synaptic parameter *lp* and a global connectivity *cp*. The values of these parameters for each participant are determined based on the features extracted from their EEG recordings. Discrimination between the HC and MCI groups is performed in the network features' space. Partitioning of the SCD group is performed in the network features' space. AD, Alzheimer's disease; *cp*, connectivity parameter; EEG, electroencephalography; FC, functional connectivity; HC, healthy condition; *lp*, local parameter; MCI, mild cognitive impairment; SCD, subjective cognitive decline; TVB; The Virtual Brain.

underwent an exhaustive neuropsychological screening (see Supplementary Materials) to determine the magnitude of their cognitive complaints. Based on the results of these analyses we divided the initial sample into two groups: (1) patients classified as SCD ($n = 58$),[3] and (2) patients classified as MCI ($n = 44$), following the National Institute on Aging–Alzheimer's Association (NIA-AA) criteria for MCI diagnosis.[4] As a control group, we also included healthy subjects (HC, $n = 17$) who volunteered to enroll in the study. The study was approved by both the Committee on Human Experimentation of the Careggi University Hospital and the local Institution Review Board ("Comitato Etico di Vasta Centro", reference: 15691oss). Before experimentations we collected written consent from all participants. All procedures related to living human participants experimentation were done in accordance with both specific national laws and the ethical standards of the Committee on Human Experimentation of the institution, in accordance with the Helsinki Declaration of 1975.

2.2 | Candidate biomarkers of disease progression in EEG

EEG recordings and pre-processing are discussed in detail in another work from our group.[13] Briefly, we recorded EEG at rest, with patients resting on a chair in a comfortable position. We used the 64-channel Galileo-NT system (EB Neuro S.p.A.), using as montage the extended 10/20 system. The sampling rate for unipolar signal recording was 512 Hz. The EEG recording session comprised a eyes-closed acquisition of 10 min, with a subsequent alternation of eyes-opened and eyes-closed periods (3 minutes each). This alternation of eyes-opened/eyes-closed states was repeated twice. We monitored electrode impedances during recording, with the requirement of being in the range between 7 and 10 kΩ. We used only the 10 minute eyes-closed acquisition for the analyses reported herein.

The candidate biomarkers for disease progression (EEG features) were extracted from two main attributes of EEG recordings at rest: FC and whole-scalp power spectral density (PSD). FC was estimated by computing envelope correlation[21] between electrodes. Envelope correlation is calculated as the Pearson correlation between couples of orthogonalized electrode signals. Briefly, the common phase between the two time series is first computed by Hilbert transformation of the signals and is then subtracted, thus avoiding spurious interactions due to the poor spatial resolution of electrophysiological recordings.[22] We computed envelope correlation for delta, theta and alpha bands, and for the whole 0.5–45 Hz range, to study the change in significant broadband connections.[23–25] FC values were tested for significance and only values larger than half of the average value of FC over all participants were kept.[26] The features extracted as candidate biomarkers for each patient from the FC data were as follows: (1) mean and standard deviation of broadband FC (BFC) values over all electrode pairs; (2) count of relevant connections; and (3) average connectivity in the delta, theta and alpha ranges. The PSD was estimated by a fast Fourier transform algorithm, using the Welch method with Hannning windowing[27] with non-overlapping segments, and a resolution of 0.5 Hz was used in both cases. Coherent with previous

literature on cognitive decline,[11,12,22,28] features extracted as candidate biomarkers from PSD were as follows: (1) alpha/delta ratio, (2) alpha/theta ratio, (3) ratio of alpha power over combined lower (delta and theta) frequency bands (A/LF ratio), and (4) individual alpha frequency. Beta and gamma were excluded from PSD analysis since values in these ranges are orders of magnitude smaller and more disperse than in the lower frequency bands.

2.3 | Biomarkers selection

We then selected the best candidates among the FC and PSD features introduced in the previous section. This was done by studying the mutual information between such features and the considered diagnostic conditions (HC, SCD, MCI). We computed the mutual information for each feature f about the group g according to the equation:

$$I(c,f) = \sum_{\substack{g\in \text{groups};\\ f\in \text{features}}} p_{(\text{groups,features})}(g|f)\log\frac{p_{\text{groups, features}}(g|f)}{p_{\text{groups}}(g)\,p_{\text{features}}(f)}, \quad (1)$$

where g is the diagnostic group, and f one of the features of the set *features*. The term $(g|f)$ represents the conditioned probability of observing the feature value f given the pertinence of the participant to group g. The two most informative EEG features, one computed from the FC and one from the PSD of the recorded signals (see above) were then selected for classification. See Supplementary Methods for further information.

The two features selected as most informative were used as experimental classifying features in the machine learning pipeline (see below), constituting the so-called "feature space."

2.4 | Classification algorithm

We then tested several machine learning algorithms to perform a binary classification between HC subjects and MCI patients based on the EEG features identified in the previous section. Hyperparameters were optimized by means of nested cross-validation.[29] Performances in discriminating HC and MCI were evaluated in terms of both accuracy and F1 score.[29] This allowed us to pick the best classifying algorithm among the ones we considered (see Figure S1). In a second set of analyses, we used the selected algorithm (ie, the random forest) to classify SCD patients in a semi-supervised fashion. Using MCI patients and HC subjects as a training set, the random forest algorithm divided the bidimensional feature space into two regions, one for the HC group and one for the MCI group. We then checked, for each of the SCD patients, the region in which they were located. In this way SCD patients were partitioned into those closer to HC (SCD→HC) or closer to MCI (SCD→MCI) according to their EEG features. Our hypothesis was that the SCD→MCI patients may present a greater neurodegeneration severity than SCD→HC patients. We then tested this hypothesis and the predictivity of the algorithm by assessing its performance in identifying SCD patients carrying biological hallmarks of the disease, strictly linked with the presence of neurodegeneration (see next subsection). We computed the performance scores with relative confidence values by bootstrapping 100 times the experimental distribution, deriving the range with 95% confidence level ($p < 0.05$) with the Clopper-Pearson method.

2.5 | CSF analysis and follow-up

A subset of 23 SCD patients underwent a lumbar puncture to analyze the CSF for the presence of biological hallmarks of AD pathology such as amyloid beta (Aβ)42, the Aβ42/Aβ40 ratio, t-tau and p-tau, with cutoff values determined from the Fujirebio guidelines.[30] Patients were rated according to the amyloid, tau, neurodegeneration (A/T[N])) system[31] and divided between carriers of AD biomarkers (CSF+, $n = 8$) and noncarriers (CSF−, $n = 15$). We then compared the percentage of carriers (CSF+ patients) in the two subgroups of SCD (SCD→MCI and SCD→HC; see previous subsection), according to both the EEG-based algorithm and the network-features based algorithm. Moreover, up to now we performed follow-up screening at 1 year for the first 20 SCD patients, checking for possible conversion from SCD to MCI.

2.6 | Cortical model

Healthy cortex was modelled in the TVB framework. The cortex was modelled as a network of 76 interacting regions. The mesoscopic activity of the regions was modelled with the Jansen-Rit neural mass model.[32] The Jansen-Rit model depicts the voltage fluctuations due to neuronal activity in cortical structures with a mean-field approach. Cortical regions are depicted as an ensemble of three subpopulations each: one population is of pyramidal cells (excitatory), one is of stellate cells (excitatory), and the last is of inhibitory interneurons. Mathematically, the activity of these subpopulations, for each node, is given by the solutions of a set of stochastic differential equations. The stochastic term is given by the input injected in each region, which has a source of additive stochastic noise (see below). The thus obtained activity is then passed as input in the equations of other regions, connected to the source region by the rules specified by the structural connectivity matrix. The equations of the model are:

$$\begin{cases} \frac{d}{dt}y_0(t) = y_3(t); \frac{d}{dt}y_3(t) \\ \qquad = \frac{A}{\tau_e}\,\text{Sigm}\left[y_1(t) - y_2(t)\right] - \frac{2}{\tau_e}y_3(t) - \left(\frac{1}{\tau_e}\right)^2 y_0(t) \\ \frac{d}{dt}y_1(t) = y_4(t); \frac{d}{dt}y_4(t) \\ \qquad = \frac{A}{\tau_e}\left\{p(t) + C_2\text{Sigm}\left[C_1 y_0(t)\right]\right\} - \frac{2}{\tau_e}y_4(t) - \left(\frac{1}{\tau_e}\right)^2 y_1(t) \\ \frac{d}{dt}y_2(t) = y_5(t); \frac{d}{dt}y_5(t) = \frac{B}{\tau_i}C_4\text{Sigm}\left[C_3 y_0(t)\right] - \frac{2}{\tau_i}y_5(t) - \left(\frac{1}{\tau_i}\right)^2 y_2(t) \end{cases}, \quad (2)$$

where y_0, y_1, and y_2 are the post-synaptic potentials of respectively the pyramidal, stellate, and interneuron populations, and y_3, y_4 and y_5 are their derivatives. The term $p(t)$ is the input written as a firing rate, that

is, the combination of the activity of other regions $\mu(t)$ and a stochastic term $\eta(t)$ that models the physiological noise: $p(t) = \eta(t) + \mu(t)$. The stochastic term $\eta(t)$ is an additive, Gaussian white noise, equal for all regions. The Sigmoid term represents the physiology-inspired nonlinear gain function that transforms the average population post-synaptic potential into a mean firing rate:

$$\text{Sigm}(v) = \frac{v_{max}}{1 + e^{r(v-v_0)}},$$

where νmax is the maximum firing rate of the population, ν_0 is the value of the potential for which there is a 50% firing rate, and r is the sigmoid slope at ν_0. The term ν_0 is also referred to as the excitability parameter of the population. We defined a model to describe the dynamics of each single node of the network, and then we linked these nodes by using a structural connectivity matrix, in which each couple of regions is characterized by a connective weight C_{weight} that mathematically transcribes the number of axonal fibers connecting the regions, and a distance between regions called C_{length} that describes the length of the fibers. In the model, C_{weight} determines the directed coupling strength between two nodes. The higher this value is, the more the activity of a region can influence the activity of other regions by increasing the value of $\mu(t)$ in the input equation. Both the model and the connectivity matrix we utilized come from the TVB framework.[33] In particular, the structural connectivity matrix and the cortex parcellation are derived from the standard TVB atlas, which combines high precision and reliability.[33] The weights C_{weight} of the TVB connectome are assigned integer values ranging from 0 to 3, that transcribe null ($C_{weight} = 0$), weak ($C_{weight} = 1$), medium ($C_{weight} = 2$), and strong ($C_{weight} = 3$) anatomical connections. The connectivity constants $C_{1,2,3,4}$ are proportional to the number of synapses that link the subpopulations together. The constants A and B, expressed in mV, are the maximal amplitude of the post-synaptic potentials for excitatory and inhibitory neurons. τ_e, τ_i, expressed in ms, are the time constants of excitatory and inhibitory population, which lump together dynamic features such as delays of the synaptic transmission and the delay in signal transmission. These last two parameters are those that we altered in order to depict the progression of the disease, and also the major reason why we chose this model, due to the fact that tuning the $\tau_e/\ \tau_i$ ratio is a simple yet highly effective way of implementing the excitation/inhibition imbalance recurrent in AD.[34] Model parameters are summarized in Table 1. FC was computed for simulated EEG as the Pearson correlation between brain regions' activity. PSD analysis was performed as we did for experimental signals.

2.7 | Disease progression model

We modeled the progression of pathology with two quantities: a connectivity parameter (*cp*) of global network connectome degeneration and a local parameter (*lp*) of regional synaptic degeneration. These quantities describe respectively the alteration of white matter fiber, in terms of both white matter atrophy and neuroplasticity,[35,36] and the degeneration of synaptic transmission (mainly excitation/inhibition imbalance)[20] according to the equations:

$$C_{\text{weight}} \rightarrow \begin{cases} C^{HC}_{\text{weight}} - cp \times C^{\text{th}}_{\text{weight}}, & \text{if } C_{\text{length}} > C^{\text{th}}_{\text{length}} \\ C^{HC}_{\text{weight}} + cp \times C^{\text{th}}_{\text{weight}}, & \text{if } C_{\text{length}} < C^{th}_{\text{length}} \end{cases}, \quad (3)$$

$$\begin{aligned} \tau_i &\rightarrow \tau_i^{HC} + lp \times \left(\tau_i^{\max} - \tau_i^{HC}\right) \\ \tau_e &\rightarrow \tau_e^{HC} + lp \times \left(\tau_e^{\min} - \tau_e^{HC}\right), \end{aligned} \quad (4)$$

where C^{th}_{weight}, τ_i^{max}, and τ_e^{min} are the extremal values of the highlighted quantities, and are $C^{th}_{weight} = 2$, $\tau_i^{max} = 40$ ms, $\tau_e^{min} = 8.9$ ms, deduced from biophysical constraints.[32,33] Arrows represent the modification of original values to model disease progression. Both *cp* and *lp* are range between 0 and 1, with 0 being the healthy and 1 being the most severe condition.

Note that we introduced, alongside excitation/inhibition imbalance and white matter fibers atrophy, a model of the correcting mechanisms operated by the brain in order to cope with the disease, such as synaptogenesis and neural plasticity.[36–38] This effect is modelled as an increase in short range connection (ie, an increase in connective weights of the structural connectivity matrix) with initially impaired regions, that is introduced along with the reduction in long range connections implemented for the same regions (Equation 3). The discrimination between short and long connections is made on the length of axonal tracts connecting the regions, C_{length} with short (long) connections existing between regions that are separated by a distance smaller (greater) than a threshold, that we deduced to be equal to $C^{max}_{length}/3$ from anatomical considerations of the utilized connectome.[33] AD appearance is not ubiquitous in the brain, and there is a subset of cortical regions in which the disease spreads significantly faster than in others.[39] To model this spreading anisotropy we induced the connectome and τ_i alterations only in a subset of regions, mostly temporal/entorhinal regions taken from well-known Braak stages, while τ_e modifications appear in the whole cortex (Equation 4).

These initially impaired regions are orbitofrontal and polar regions of prefrontal cortex, and the polar, central, inferior, and ventral temporal cortex.

2.8 | Brain signal simulation

Regional activity is obtained by solving the set of stochastic differential equations given by the Jansen-Rit model (Equation 2), which are computed by means of the stochastic Heun method,[40] with a timestep of 0.1 ms. For each run, we simulated 10 seconds of local electrophysiological activity, with a resolution of 1 ms.

2.9 | Tuning the model to patient-specific EEG features

We estimated *lp*s and *cp*s for each individual patient as follows. First, we computed in simulated data for the A/LF ratio and average BFC as

TABLE 1 Model parameters.

Parameter label	Description	Unit of measure	Value
A	Maximum excitatory post-synaptic potential	mV	3.25
B	Maximum inhibitory post-synaptic potential	mV	22.0
τ_e	**Excitatory time constant**	ms	10
τ_i	**Inhibitory time constant**	ms	20
*v*0	Voltage threshold for which a 50 % firing rate is achieved	mV	6.0
νmax	Maximum firing rate of neural population	s−1	0.0025
r	Steepness of sigmoidal transfer function	mV−1	0.56
*C*1	Average probability of synaptic contacts in the feedback excitatory loop	pure number	1.0
*C*2	Average probability of synaptic contacts in the slow feedback excitatory loop	pure number	0.8
*C*3	Average probability of synaptic contacts in the feedback inhibitory loop	pure number	0.25
*C*4	Average probability of synaptic contacts in the slow feedback inhibitory loop	pure number	0.25
η	Mean input noise	s−1	0.22
μ	Mean input from other regions	s−1	0.22
Cweight	**Connective weights with other nodes**	pure number	0–3
Clength	Distance from other nodes	mm	0–138

Note: Quantities in bold are those modified in order to depict Alzheimer's disease effects.

a function of *lp* and *cp*. We did a grid-search by changing the values of both *lp* and *cp* in 50 linear steps between 0 and 1. We thus obtained the two matrices of simulated EEG features *A/LFmod*(*lp*, *cp*) and *BFCmod*(*lp*, *cp*).

We also computed the vectors *A/LFexp* (*subj*) and *BFCexp* (*subj*), containing respectively the values of the A/LF ratio and of the BFC for each participant. We then normalized both the experimental and the simulated features between their minimum and maximum values.

We then computed the total weighted Euclidean distance between the experimental values of the EEG features of each participant and each value of the simulated features matrices:

$$\mathrm{D(subj, [}lp, cp\mathrm{])}^2 = \mathrm{Distance_{BFC}}^2 + W \times \mathrm{Distance_{A/LF}}^2,$$

where the quantities $Distance_{A/LF}$ and $Distance_{BFC}$ are defined by the equations:

$$\mathrm{Distance_{A/LF}} = \mathrm{A/LF^{exp}(subj)} - \mathrm{A/LF^{mod}}(lp,cp),$$
$$\mathrm{Distance_{BFC}} = \mathrm{BFC^{exp}(subj)} - \mathrm{BFC^{mod}}\ (lp,cp).$$

The distance operator allows to select the optimal values of *cp* and *lp* for each patient. This is done by finding the combination of *cp* and *lp* that minimizes the squared difference between experimental values of A/LF and BFC (the *A/LFexp* (*subj*) and *BFCexp* (*subj*) vectors), and their simulated counterparts (the *A/LFmod*(*lp*, *cp*) and *BFCmod*(*lp*, *cp*) matrices). The purpose of the parameter *W* is to find the weighted distance from the experimental EEG features that, when minimized, identifies the distribution of network features that best classifies HC subjects and MCI patients. Each value of *W* univocally identifies a distribution of *cp* and *lp*. We determined the optimal *W* by looking for the distribution that maximized the HC−MCI classification performance in the *W* value range 0.005−16. We found $W = 12$ to be the best weight value, and we then determined the *lp*−*cp* combination for each patient, by minimizing the distance with that value of *W* as the weight. By identifying these value pairs, we unequivocally found the combination of network features that best describes the given patient in terms of the relevant features computed from their EEG. We also checked the robustness of this procedure, by applying a gaussian random noise to the experimental *A/LFexp* (*sub*) and *BFCexp* (*sub*) values used to determine the best fitting parameters. The noise was distributed for each feature in an interval centered in its original value, with the interval length

given by 10% of the same value. We then recomputed the network features from the new distribution of EEG features. For better clarity, the pseudocode for the fitting function is reported in Supplementary Materials.

2.10 | Classifying patient conditions with network parameters

The classification of the participants' condition described in Section 2.4 (Classification algorithm) was then repeated based on the network parameters *lp* and *cp* rather than the EEG features *A/LFexp* and average alpha FC. First, the patients' specific values of *lp* and *cp* were used to discriminate between HC and MCI. Then, SCD patients were assigned by the same algorithm either to the HC or to the MCI category as we did for EEG features. Finally, to check if our model could determine the degree of structural alterations due to disease progression, we compared the percentage of CSF+ patients in the two subsets identified by the classifier (see Section 2.5, CSF analysis an follow-up). This was done to assess if our proposed classification and prediction could outperform the one based on standard experimental data.

2.11 | Outlier management

Outliers, defined as participants whose computed features were more than four standard deviations away from the mean value, were discarded from both the statistical analysis of the dataset and from the classifying pipeline. We did not find outliers in the EEG features, while we found one in the network features of the HC group, reducing the group size to $n = 16$ subjects.

2.12 | Graph theoretical analysis

To link the functional and dynamic non-linearities observed during the simulated structural connectivity degeneration, we performed a graph theoretical analysis of the structural matrices of the model while varying the *cp* parameter. We utilized the Randic index,[41] a quantity that has already been used in studies concerning AD.[42]

This quantity, defined as the sum of $\frac{1}{(C_{weight}(i,j)C_{weight}(j,i))}$ out of every possible (i, j) pair, is anti-correlated with the tendency of each node to be linked with nodes of similar degree, the so called "rich-club phenomenon."[43] The rich-club phenomenon is known to apply to the connections in the healthy cortical network.[43] We studied the evolution of the Randic index during the progression of the disease, by computing this quantity for every value of *cp*, comparing the results with the variation of both *A/Lfmod* and *BFCmod* according to the same variable. We also investigated the Randic index evolution in a network model with a random structural connectivity matrix, that is, with random connective strength $C_{weight}(i, j)$ between regions. By increasing *cp* in the random network model, and by computing the Randic index for each *cp* value, we could check if the non-linearities observed in the original network depends solely on *cp* or if they could derive also from the non-trivial network topology.

2.13 | Statistical analysis

Distribution normality was assessed by using the Shapiro–Wilk test. For approximately normally distributed variables ($p > 0.01$) we used a one-way analysis of variance (ANOVA) *f*-test, otherwise we chose the Kruskal–Wallis non-parametric test to compare the three groups. Similarity in distribution of connective weights was assessed with the Kolmogorov–Smirnov test. Post hoc analysis was conducted by Bonferroni correction after pairwise comparisons between groups. We also tested the effect size by means of Cohen's *d*. Only differences with $d > 0.50$ (large effect size) were listed as significant. All tests were two-tailed, except for the test for the significance of the CSF+ prediction, which was a one-tailed test on the binomial distribution with 50% probability as the null hypothesis, and for the significance test for the performance metrics of the machine learning pipeline. The confidence ranges of performance metrics for the MCI versus HC classification were assessed by generating a null distribution with the bootstrap test with 250 iterations and by taking the 2.5% and 97.5% percentiles ($p = 0.05$). For the confidence ranges of the CSF prediction, since the sample sizes were smaller than in the previous case, we opted for the Clopper-Pearson method. Statistical analysis was implemented in Python using the standard Scipy package.

3 | RESULTS

3.1 | EEG features in early stages of AD

We recorded EEG signals at rest from patients with MCI and SCD, along with HC subjects (see Methods for details). We first classified participants in these groups based on EEG features, extracting for each one the PSD and FC between pairs of electrodes, two known EEG biomarkers of AD.[11,12]

The whole-scalp PSD presented significant differences across the three groups (see Methods) only within the alpha band (8–12 Hz) and within the low-beta range (12–20 Hz) ($p < 0.05$, one-way ANOVA with Bonferroni correction, Figure 2A). In both ranges the PSD was higher for the HC than for the SCD, and for the SCD than for the MCI groups. The opposite ranking was observed for the delta (0.5–4 Hz) and theta (4–8 Hz) bands, although intergroup differences were not significant. We computed the information about the three groups carried by other spectral EEG biomarkers based on standard frequency bands (see Methods), and we found the alpha/(delta + theta) power ratio (A/LF ratio) to be the most informative EEG spectral feature (see Figure S1a). However, this ratio was not significantly different across groups (Kruskal–Wallis test, statistic = 2.86, $p = 0.24$, Figure 2B). We computed FC (see Methods) over frequency bands, along with BFC[23–25] (see Figure S2). Mean BFC values did not differ significantly between groups (0.072 ± 0.037 for the HC group, 0.071 ± 0.035 for the SCD

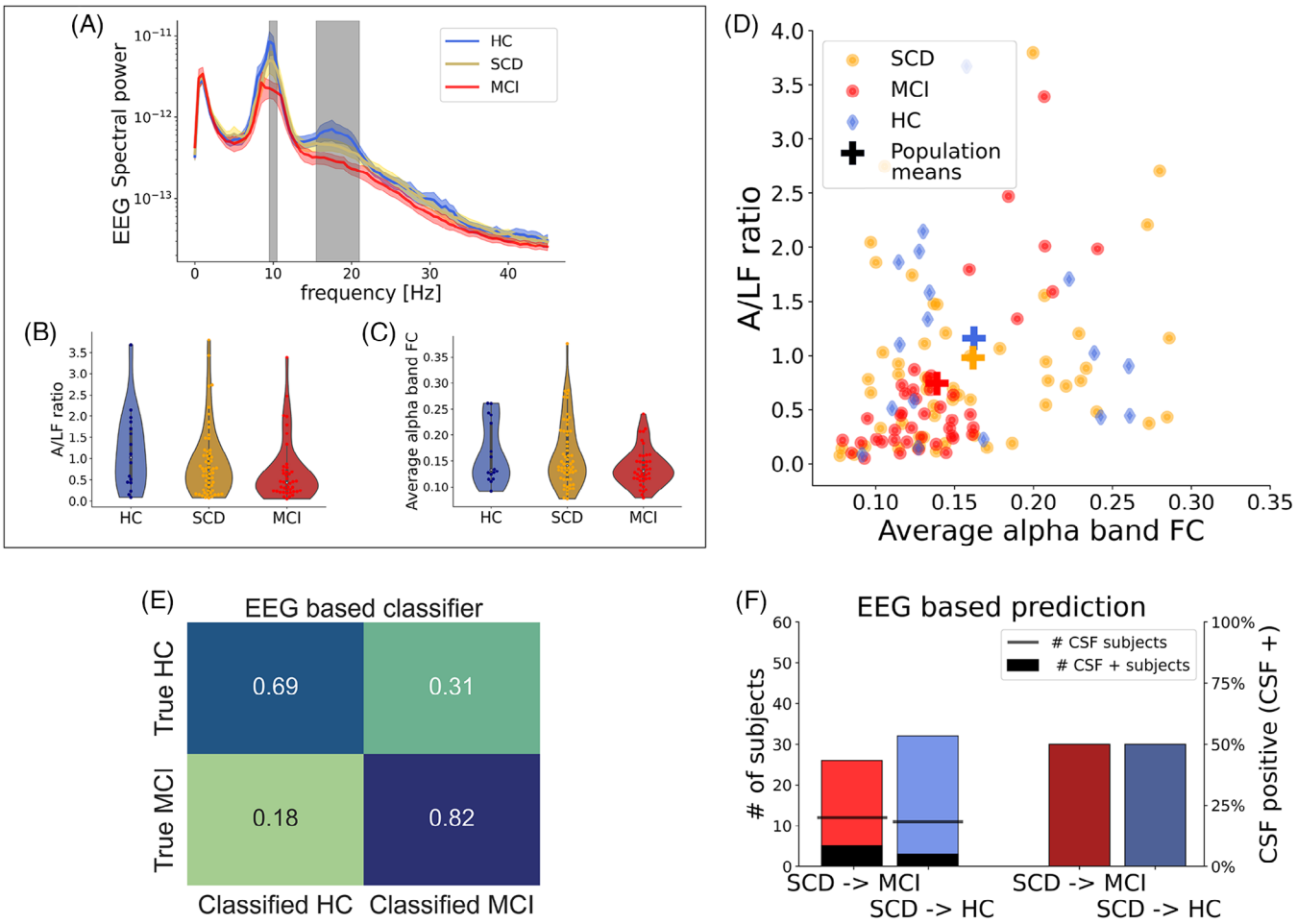

FIGURE 2 Decoding of patients' condition and prediction based on EEG features. (A) Mean PSD for all groups (HC, MCI, SCD), shaded area around PSD curves representing the standard error of the mean. Gray bars indicate frequency ranges displaying significant differences ($p < 0.05$) across groups. (B) Ratio between power in the alpha band and lower frequencies (A/LF ratio) for the three groups. (C) FC in the alpha band (alpha FC) for the three groups. (D) Combined representation of A/LF ratio and average alpha FC for each participant in each group. Cross-shaped markers indicate the mean values of the three groups. (E) Confusion matrix for HC versus MCI for optimal classification algorithm based on EEG features (F) Left: SCD patients classified as HC (light red) and MCI (cyan) with the same classification algorithm used in panel D. Black bars indicate the numbers of patients whose CSF was positive to AD biomarkers (CSF+) within each set. Right: Percentages of CSF+ patients for each category (brown red and dark cyan). AD, Alzheimer's disease; CSF, cerebrospinal fluid; EEG, electroencephalography; FC, functional connectivity; HC, healthy condition; MCI, mild cognitive impairment; PSD, power spectral density; SCD, subjective cognitive decline.

group, and 0.069 ± 0.031 for the MCI group). We then binarized the BFC setting using as threshold the mean BFC value[26] to study the differences in the number of relevant functional connections between groups (see Methods). The MCI group displayed an average decrease of significant connections compared to HC subjects (17.8% of connections present in the HC group are lost in MCI patients while only 7.6% of the connections present in the MCI group are gained, see Figure S3a left). Surprisingly, comparing the SCD and HC groups, the overall prevalence was an increase in the number of significant connections (11.9% gained vs 6.9% lost, Figure S3a center). Connections were instead lost in the MCI group compared with the SCI group (18.2% lost vs 2.95% gained, Figure S3a right). This suggests a non-monotonous progression of FC weakening across cognitive decline severity.[36–38] We then computed the amount of information carried about the three groups by the EEG FC biomarkers of AD (Figure S1b). The most informative was the average alpha band FC even if no significant difference was present between groups (Figure 2C, Kruskal–Wallis test, statistic = 5.70, $p = 0.057$). The shape of the BFC distribution, instead, significantly changed across groups (Kolmogorov–Smirnov test, HC vs SCD test = 0.077, HC vs MCI test = 0.10, SCD vs MCI test = 0.038, $p << 0.0001$ across all groups), with the largest variability being present in SCD patients (the coefficient of variation was 0.051 for SCD, and 0.047 for both HC and MCI). We tested the classification performance of combinations of PSD and FC features in discriminating between HC and MCI (Table 2) using the random forest algorithm as it outperformed other approaches (Table S1). The strongest classification was based on the average alpha band FC and A/LF ratio (see scatter plot in Figure 2D), achieving an accuracy of 78% [69%–86%] (alpha = 0.05 computed from bootstrap distribution, see Methods), with an F1 score of 0.75 [0.68–0.83] and recall (fraction of MCI patients correctly

TABLE 2 Top four classifier performances trained with combinations of EEG spectral and FC features.

EEG features	Classifier	Accuracy	F1 score
A/LF ratio—FC alpha band average	Random Forest	0.78	0.85
	SVM, rbf kernel	0.68	0.73
	SVM, polynomial	0.70	0.72
	SVM, linear	0.64	0.57

Note: Other algorithms that we considered performed poorly in classifying MCI patients and HC subjects. These were (1) decision tree, (2) native Bayes, (3) nearest neighbors.
Abbreviations: A/LF, ratio of alpha power over combined lower frequency bands; EEG, electroencephalography; FC, functional connectivity; HC, healthy condition; MCI, mild cognitive impairment; rbf, radial basis function; SVM, support vector machine.

identified) of 0.82 [0.73–0.91]. The HC–MCI inter-cluster separation was 0.46 (see Methods). We investigated whether we could discriminate SCD patients more at risk of progressing toward AD based on their similarity with MCI rather than with HC in the EEG features space. We then used the same algorithm used to discriminate between HC and MCI (using again the HC and MCI groups as a training set) to classify SCD patients in a semi-supervised fashion (see Methods). In this way SCD patients were partitioned into a subgroup classified as being closer to the HC (SCD→HC) and a subgroup closer to MCI (SCD→MCI). We checked the performance of this algorithm in predicting the presence of biological hallmarks of AD pathology. We did this by comparing the results of CSF markers (strongly related to structural alteration,[7] see Methods) for the two subgroups identified by the algorithm. However, the number of CSF+ patients was the same in the SCD→MCI and SCD→HC subgroups (4 vs 4, Figure 2F). We computed the accuracy of the algorithm in discriminating CSF+ and CSF− (Clopper-Pearson method, see Methods), finding a value of 48% [38%–58%]. The F1 score was equal to 0.40 [0.30–0.50], and the recall (fraction of CSF+ patients correctly identified) was 0.50 [0.39–0.61] (see Methods). Finally, at 1 year follow-up, three of the SCD patients transitioned to MCI. We checked whether the algorithm could predict such transition (by correctly placing converted patients in the SCD→MCI subgroup). Only one of them (1/3) was correctly identified. This suggests that decoders based on standard PSD and FC EEG features display a low segregation between MCI and HC and could not be used to provide an outlook on SCD patients' condition.

3.2 | Multiscale cortical network model of progression to AD

To overcome the limitations of EEG in assessing neurodegeneration severity, we hypothesized that reconstructing from the model the specific circuital changes induced by the early stage of AD-type dementia in each participant (Figure 1, bottom) could highlight parameters enabling a more accurate classification of patients than the one allowed by EEG features. We started from the model of the healthy cortex available in the EBRAINS TVB platform (see Methods). Then we modeled the neural circuit correlates of the onset of AD-type dementia considering changes at the level of both local dynamics and global connectivity (Figure 3 and Methods). Briefly, structural connectivity degeneration was modeled by considering both a decrease in long-range connections due to white matter atrophy and an increase in short-range connections due to neuroplastic mechanisms (see Methods). Synaptic degeneration was accounted for by modeling alterations in inhibitory and excitatory synaptic time scales. These two processes are summarized by two network features: *cp* for connectivity degeneration effects and *lp* for synaptic degeneration effects (see Equations 3 and 4 in the Methods and in Figure 3).

We first assessed whether the model was able to reproduce the alterations of EEG features (PSD and FC) observed in the SCD and MCI groups. For suited pairs of *cp* and *lp* values (see Methods) the model was able to reproduce qualitatively both connectivity and spectral features of HC, SCD, and MCI from EEG recordings. The combination of *cp* and *lp* parameters reproducing experimental features was $cp_{HC} = 0.48$ and $lp_{HC} = 0.30$ for HC, $cp_{SCD} = 0.64$ and $lp_{SCD} = 0.46$ for SCD, and $cp_{MCI} = 0.98$ and $lp_{MCI} = 0.84$ for MCI, coherent with the expected positive correlation between the magnitude of network features and the severity of the condition. For these network feature pairs the model displayed the experimentally observed decrease in alpha band in the SCD and MCI groups with respect to the HC group, as well as the decrease in beta band power observed in MCI patients (12.5% ± 2.6 power loss with respect to the HC group values for the MCI group in the beta band, and 10.3% ± 2.1 and 41.3% ± 8.3 power loss for the SCD and MCI groups, respectively, with respect to the HC group values in the alpha band). Coherently with the experimental results, the A/LF ratio decreased for larger values of network features (Figure S3a).

Since we computed FC in the network model between cortical regions rather than between electrodes, we compared the simulated network FC with the broadband envelope correlation computed from EEG signals, as previous studies suggested that this measure is suited to study functional connections between source regions.[44] Note that BFC was a highly informative EEG feature discriminating the groups (Figure S1). For the same parameter values reproducing observed spectral modulations the model also displayed the same observed differences in FC across groups (SCD vs HC: 8.3% lost vs 12.1% gained connections; MCI vs SCD: 15.5% lost vs 6.95% gained connections; MCI vs HC: 13.1% lost vs 8.30% gained connections, Figure S3b,c). Coherent with the experimental recordings analysis, the average BFC displayed similar values across groups (0.074 for HC and SCD, and 0.071 for MCI). Overall, the network model was able to capture both variation in the low frequency spectrum and the non-linearity in connectivity progression associated with different conditions in EEG recordings.

3.3 | Relationship between network features and EEG features

We then investigated the relationship between the average BFC and A/LF ratio in simulated data and the underlying network features

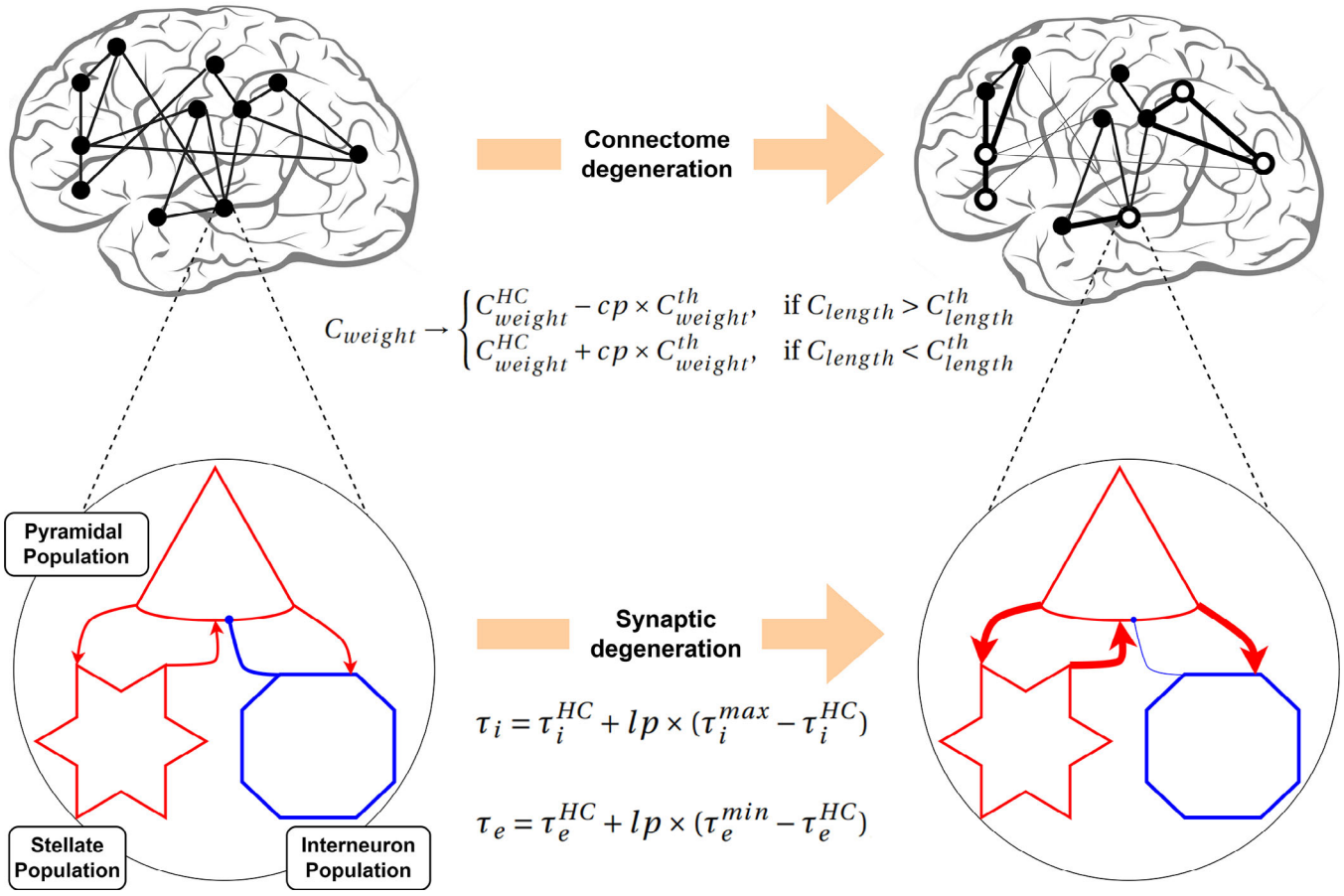

FIGURE 3 Outline of the model of AD-related structural alterations. Top row: A macro-scale *cp* describes the degree of alterations in structural connectivity, through linear strengthening of short-range and weakening of long-range connections. Thickness of the lines is proportional to connection strength; white nodes are those affected by AD-type dementia. Bottom row: A meso-scale *lp* describes the degree of synaptic degeneration through a local slowing of inhibitory synapses, alongside a global quickening of excitatory synapses. This leads to hypo-inhibition in the regions impaired by the disease, along with a milder but ubiquitous hyperexcitation. AD, Alzheimer's disease; *cp*, connectivity parameter; lp, local parameter.

modeling the degeneration process *cp* and *lp* (Figure 4). We simulated brain signals as a function of both *lp* and *cp* and we computed the associated BFC and A/LF ratio.

BFC (Figure 4A) increased with *lp* for all values of *cp* (Figure 4B). The relationship between BFC and *cp* depended instead on *lp*: when *lp* was high BFC displayed a peak value for intermediate values of *cp*, suggesting a non-linearity of BFC during progression toward AD, whereas when *lp* was low BFC increased monotonously (Figure 4C). To understand how this was related to the structure of the network, we measured the assortativity of the network by computing its Randic index (see Methods and[41,42]) as a function of *cp* (Figure 4D). The Randic index displayed a nonlinear trend, with values even lower than those found in the healthy case for early stages of the disease progression, followed by a steep increase for high values of *cp* increases. The Randic index links the state of structural and functional alterations and could explain the non-linearity observed in the FC measurements in EEG. Our model suggests that the gradual decline of long-range connections and the enhancement of connections between nearby affected regions could cause a temporary increase in assortativity. This is then followed by a sharp decrease due to the worsening state of long-range connections. Our findings suggest that the topology of a healthy cortical network is the source of observed non-linearities indicated by the Randic index. We tested this hypothesis by progressively increasing the *cp* parameter, this time starting from a random structural connectivity matrix (ie, with random values of C_{weight} between regions). We found that both the simulated FC and Randic index to show monotonic evolution with the progression of the disease (increasing *cp* parameter), suggesting that the nonlinear evolution observed in experimental data stems from the complex topology of the network (Figure S4a—b).

We next investigated the evolution of the A/LF ratio when the parameters associated with AD progression are increased (Figure 4E). For high values of *lp* the ratio decreased with *cp*, while the opposite was true for low values of *lp* (Figure 4F). The increase of *lp* was instead always associated to a steep decline in the ratio.

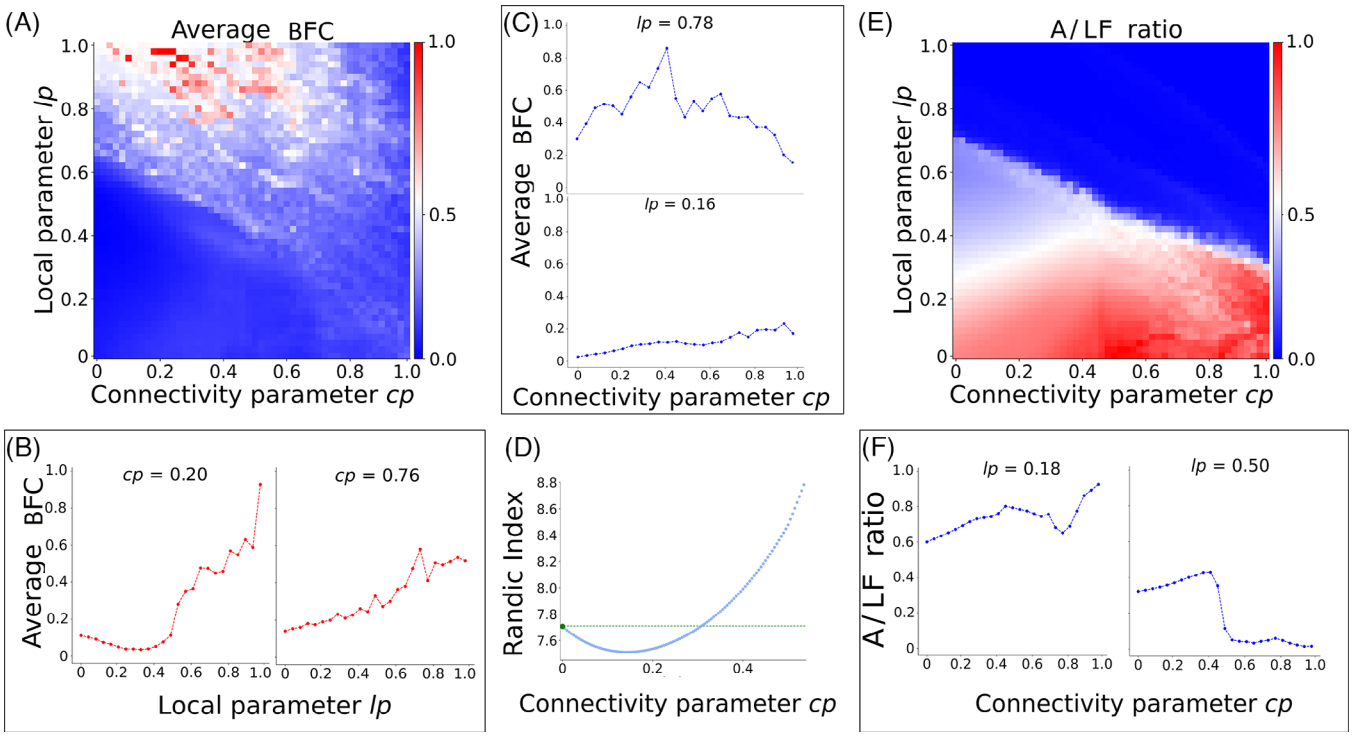

FIGURE 4 Relation between *cp* and parameters and simulated features. (A) Average BFC for the network model as a function of local and connectivity parameters, *lp* and *cp*. (B) BFC as a function of *lp* for fixed values of *cp*. (C) BFC as a function of *cp* for fixed values of *lp*. (D) Randic index as a function of *cp*, showing nonlinear evolution of network assortativity during disease progression. (E) A/LF power ratio for the network model as a function of *lp* and *cp*. (F) A/LF ratio as a function of *cp* for a fixed value of *lp*. A/LF, alpha band/lower frequencies; BFC, broad-band functional connectivity; *cp*, connectivity parameter; EEG, electroencephalography; *lp*; local parameter.

3.4 | Personalized network features lead to reliable classification and prediction of AD pathology

We finally proceeded to compute personalized network features cp_{subj} and lp_{subj} to feed them (rather than EEG features) into the classification and prediction algorithms.

We determined for each participant the subjective combination of network parameters [cp_{subj} lp_{subj}] that allowed the best reproduction of the EEG features computed from their recording. This allowed us to define for each participant a personalized network with an estimated measure of connectome degeneration, given by cp_{subj}, and an estimated level of synaptic degeneration, given by lp_{subj} (Figure 5A). The two parameters were correlated across participants for merged groups ($r^2 = 0.077$, $p = 0.002$), but correlation decreases when computed for each group ($r^2 = 0.40$ $p = 0.006$ for HC, $r^2 = 0.12$, $p = 0.008$ for SCD, and $r^2 = 0.083$, $p = 0.061$ for MCI) with a larger mean squared error (MSE) for the SCD and MCI groups (MSE = 0.12 for HC, 0.91 for SCD, and 0.62 for MCI; see Figure 5B).

We found *lp*s to be significantly smaller in HC subjects with respect to MCI (one-way ANOVA, $f = 6.17$, $p = 0.048$, with Bonferroni correction, Cohen's $d = 0.73$) but not to SCD patients (one-way ANOVA, $f = 1.73$, $p = 0.126$, with Bonferroni correction, Figure 5C). The *cp*s did not differ significantly across groups (Kruskal–Wallis test, statistic = 0.35, $p = 0.70$) (Figure 5D). We also computed for each participant the average Euclidean distance in the [cp_{subj}, lp_{subj}] space (Figure 5A) from the center of the HC group (determined by the average HC values of *cp* and *lp*). This distance was significantly smaller in HC subjects with respect to MCI (one-way ANOVA, $f = 6.56$, $p = 0.039$, Bonferroni correction, Cohen's $d = 0.61$) and to SCD patients prior to Bonferroni correction (one-way ANOVA, $f = 4.89$, $p = 0.09$, Bonferroni correction, Cohen's $d = 0.75$, Figure 5E). We also tested the robustness of this pipeline by adding a random value (generated with a Gaussian distribution) to the EEG features, checking how this random displacement influenced the [cp_{subj}, lp_{subj}] combination for each patient (see Methods). Results are shown in Figure S5, which highlights the stability of the parameter determination procedure.

The fact that network features displayed significant differences across groups is particularly relevant as this was not the case with the experimental EEG features. To assess whether this led to an improvement in the classification performance, we repeated the classification between MCI patients and HC subjects using the same algorithm utilized for the classification with EEG features (see Methods), but using only the network features (the [cp_{subj}, lp_{subj}] combination). We found an accuracy of 93% [87%–97%], with an F1 score of 0.95 [0.91–0.98] and a recall (fraction of MCI patients correctly identified) of 0.91 [0.84–0.96]. The two clusters also displayed a clear separation, $d^{mod} = 1.26$.

Since the algorithm based on network features performed better than the EEG-based one in discriminating between HC and MCI, we investigated whether it could determine the presence of

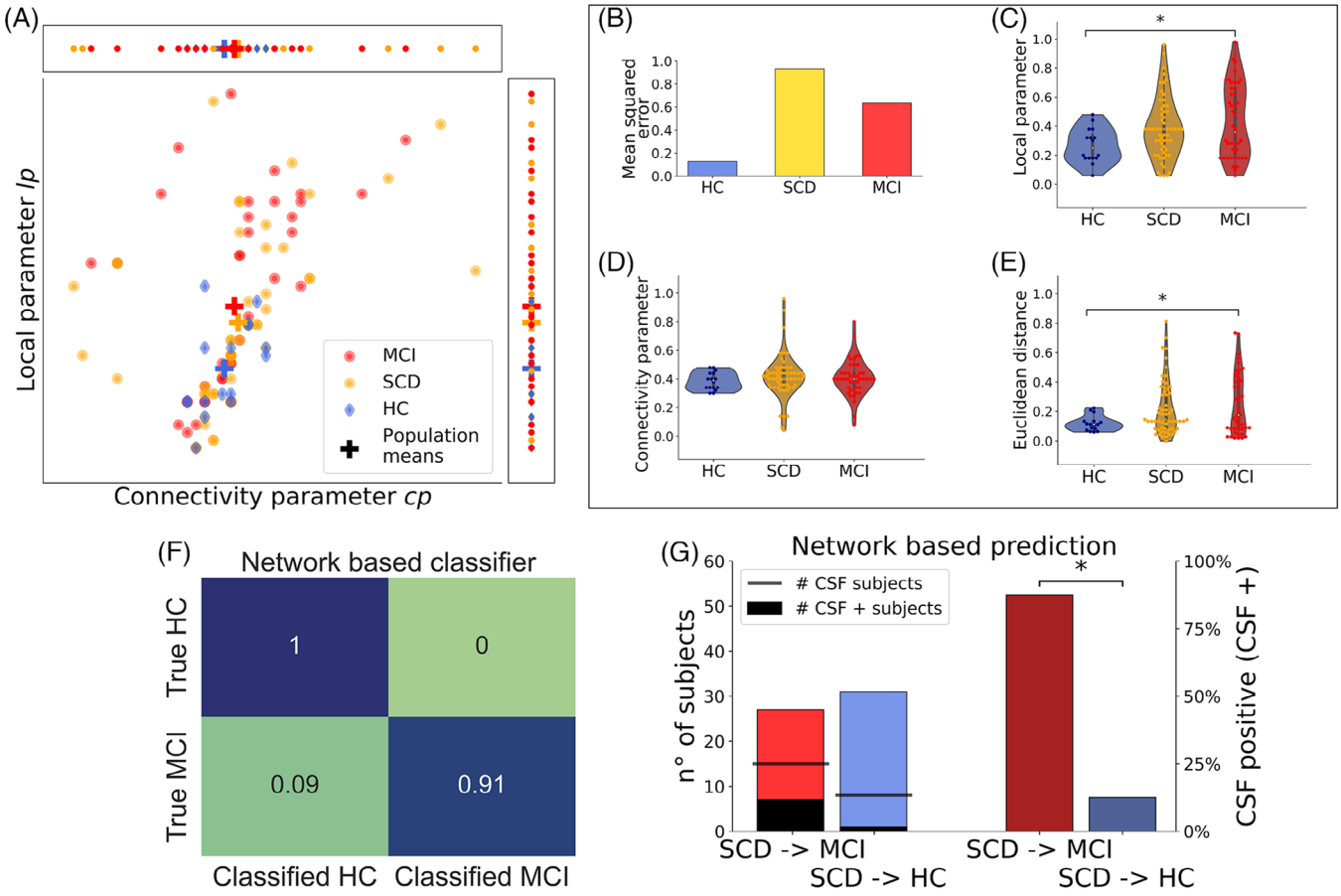

FIGURE 5 Decoding of patients' condition and prediction based on network features. (A) Combined representation of network features *lp* and *cp* for each participant in each group (HC, MCI, and SCD). Cross-shaped markers indicate the mean values of the three groups. (B) Mean squared error of the linear fit for each group. (C–E) Distribution across groups of *lp*s (C), *cp*s (D), and Euclidean distance from the healthy cluster center (E). (F) Confusion matrix for HC versus MCI optimal classification algorithm based on network parameters. (G) Left: SCD patients classified as HC (light red) and MCI (cyan) with the same algorithm used for experimental EEG features (see text). Black bars indicate the number of CSF+ patients within each set. Right: percentages of CSF+ patients for each category (brown red and dark cyan). $^*p < 0.05$ (Fisher's test). *cp*, connectivity parameter; CSF, cerebrospinal fluid; EEG, electroencephalography; HC, healthy condition; *lp*; local parameter; MCI, mild cognitive impairment; SCD, subjective cognitive decline.

biological hallmarks of AD in SCD patients, and possibly their future progression. Following the procedure applied for the EEG features-based algorithm (see Methods), we partitioned the SCD patients into SCD classified as MCI (SCD→MCI) and SCD classified as HC (SCD→HC) based on their personal network features. To test the hypothesis that the network features partition could predict biological hallmarks of AD in SCD patients, we compared the presence of CSF markers for the two SCD subgroups. We found a significatively higher number of CSF biomarker carriers in the SCD→MCI group with respect to the SCD→HC classified group (7 vs 1, Fisher test $p = 0.04$, Figure 5G). The accuracy of the partition in discriminating CSF+ and CSF− was 61% [51%–70%], the F1 score was 0.60 [0.50–0.69], and the recall was 0.87 [0.78–0.93]. These results suggest that the algorithm based on network features extracted from resting EEG signals could predict biological hallmarks of AD pathology. We also checked the performance of the algorithm based on network features in predicting converted patients, as we did for the algorithm based on EEG features. Strikingly, we found that all (3/3) patients that converted from SCD tom MCI at 1 year follow-up belonged to the SCD→MCI group identified with network features (remember that only 1/3 was identified with EEG features). This corroborates the strong enhancement in diagnostic and prognostic ability obtained by the network-driven analysis of EEG signal in comparison with standard quantitative techniques.

Overall, the network-based algorithm significantly outperformed the EEG-based algorithm in HC versus MCI classification (Figure 6, top row), while also allowing for the first time to predict biological hallmarks of AD pathology from EEG recordings, which was up to now unfeasible (Figure 6, bottom row). These results appear even more relevant if we note that converted patients showed no distinct symptomatology (being diagnosed as SCD). Note that network features replaced the EEG features, rather than being used in combination with them to enhance the performance of the classifier as done in several studies (see Discussion).

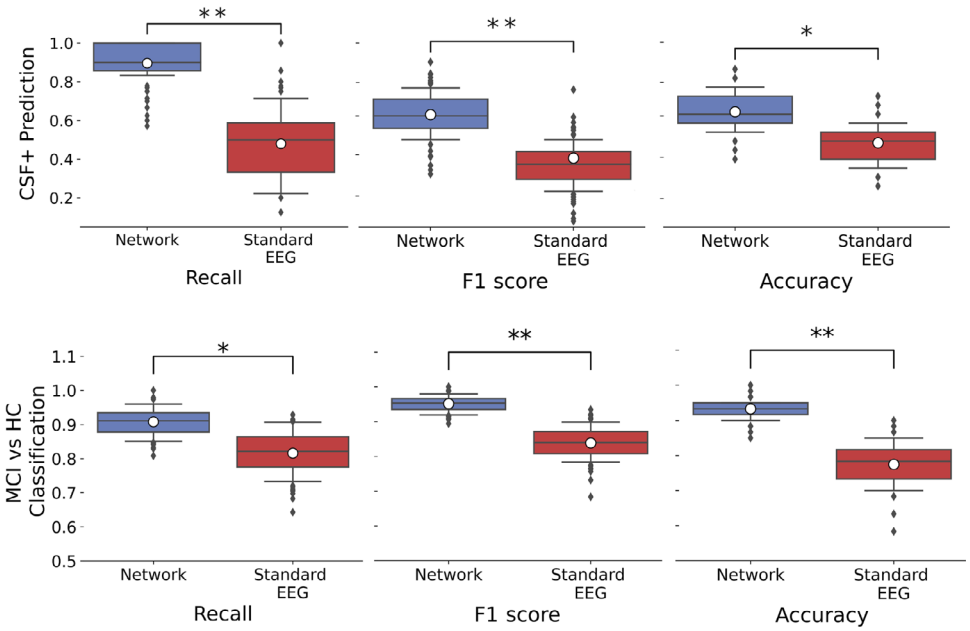

FIGURE 6 Performance comparison between EEG-based and network-based algorithms after bootstrapping. Top row: Performance on predicting the biological hallmarks of the disease in the CSF. Bottom row: Performance on classifying between MCI and HC conditions. White dots represent experimental values. Significance notation: $^{*}p < 0.05$ for (1) experimental value of EEG-based algorithm below confidence range of the network-based algorithm and (2) experimental value of network-based algorithm above confidence range of the EEG-based algorithm. $^{**}p = 0.05$ for non-overlapping confidence ranges. CSF, cerebrospinal fluid; EEG, electroencephalography; HC, healthy condition; MCI, mild cognitive impairment.

4 | DISCUSSION

We developed a computational model estimating the level of degeneration in local connections and global connectivity during the trajectory toward AD. These changes can be estimated on an individual basis combining the model with spectral and connectivity attributes of a patient's resting-state EEG recordings. Leveraging these attributes as input, machine learning algorithms demonstrated prowess in classifying early stages of AD and forecasting their progression, significantly surpassing algorithms founded solely on conventional informative EEG features. The potency of our approach stems from its innovative incorporation of knowledge concerning the course of AD-related neurodegeneration in the decoding of EEG signals.

4.1 | A patient-specific, multi-scale model of disease progression

Our model replicates salient aspects of healthy and pathological EEG recordings across varying scales, aptly encompassing the spectral and connectivity characteristics observed experimentally. The model captures several structural alterations wrought by the disease, encompassing synaptic degeneration and hyperexcitation and white matter atrophy. While an earlier work on AD modeling introduced a specific model pertaining to the decline in the alpha/theta ratio,[19] our model extends its scope to accommodate a broader array of structural modifications, thereby becoming capable of accounting for their effects on connectivity. Furthermore, we have introduced explicit representation of neuroplastic adaptive phenomena embodied as augmented short-range increases in structural connectivity within impaired regions aligning with the observed nonlinear evolution of FC as AD advances. These structural and circuital shifts, distilled into two parameters (*cp* and *lp*), calibrate the model to each patient's electrophysiological signals, thereby linking the experimentally observed EEG biomarkers with computationally determined structural parameters of neurodegeneration. Distinct from prior work such as,[19] which focused on predicting EEG features from structural changes, our endeavor prioritizes the estimate of neurodegeneration severity through non-invasive recordings, tailoring the model to the unique EEG features of each participant.

4.2 | Classification of MCI with EEG features

The model lay at the core of a clinical pipeline to estimate the severity of each patient's neurodegeneration through a quantitative analysis of their resting EEG signal. The EEG signal was processed through the model to extract biomarkers more informative than the standard EEG features. We used as benchmark for EEG analysis the performance of algorithms for the classification of MCI based on spectral and connectivity features, which are the most common tool to assess MCI conditions from EEG[11,45–52] and are even investigated as possible markers of progression to AD.[37] The results were in line with previous studies performing MCI classification with these features,[9,10,13,14,53]

but was vastly outperformed by the model-based procedure (Figure 6).

However, the range of possible EEG features extends beyond the ones we tested. Promising results have been achieved through network[54] or microstate analysis.[13,55] Moreover, EEG features collected during cognitive tasks are likely to be more informative than those acquired at rest and hence lead to a more efficient classification of EEG synchronization in MCI and AD.[56] A potential alternative approach is the automatic learning of features based on deep learning tools.[57] Novel approaches can improve not only classification with EEG features, but also improve the design of personalized models. Previous works utilized models personalized with structural scans, such as,[19] to derive novel features to support the classification of AD and MCI patients.[53,58] Besides the difference in approach highlighted in the previous section, we also note that in our case network model features replace features based on recordings in the classification algorithm, rather than being combined with them, nonetheless enabling us to obtain a much higher accuracy in discriminating healthy subjects and MCI patients.

4.3 | Model prediction of AD pathology and clinical outcome

Detecting AD at its nascent stages is pivotal, as it offers a window of opportunity for early therapeutic interventions. However, the complexity of diagnosing SCD arises from its elusive and heterogeneous nature, characterized by the absence of distinctive symptomatology.[3] Unlike clinical AD, SCD lacks the objective cognitive deficits that can be readily quantified through standardized neuropsychological assessments, rendering diagnosis reliant on subjective reports of cognitive decline from individuals themselves or their informants.

This inherent subjectivity in symptom reporting poses challenges in ascertaining the validity and specificity of SCD as a clinical entity. Our model-based approach was able to partition SCD into two subsets with a significant different presence of CSF biomarkers (currently the most reliable biomarker of AD pathology,[20] Figure 5G). The prediction of CSF biomarkers in SCD patients was never attempted before to the best of our knowledge, and in fact was unachievable when using standard quantitative EEG analysis (Figure 2F).

This constitutes the first example of prediction of biological hallmarks of AD from EEG recordings, a fortiori in pre-AD patients without evident symptomatology. Moreover, we conducted follow-up screening after 1 year to check for converted patients, finding three SCD-to-MCI conversions. Strikingly, all three SCD patients that converted were correctly identified in the SCD→MCI group by our model. These results pave the way for a novel approach to EEG analysis, which could extract from such an affordable and non-invasive technique information until now obtainable only via more complex and/or stressful exams.

4.4 | Limitations and future directions

The first limitation of our study pertains to the size of the three participant groups, and in particular the smaller size for the control group compared to the other two groups. We sufficiently minimized the bias introduced by this discrepancy in the statistical analysis by testing the effect sizes of statistical differences (see Methods). Furthermore, the CSF was analyzed only on a limited subset of patients. A larger dataset will further enable a more detailed investigation of the role played by demographic factors such as sex and age. In particular, future studies will address the possibility of using the model to disentangle between structural changes associated with healthy aging and those associated with neurodegeneration.

One of the key results of our work, namely, the fact that network features were able to correctly recall CSF+ patients in 7/8 cases (against 4/8 with EEG features), was achieved by analyzing a limited subset of 23/58 SCD patients. The results are statistically robust and the difference between the two decoding performances is significant (see Methods for details). However, to properly assess the efficacy of our approach, a multicenter study is needed and will be performed. Similarly, we reported the observation that our approach predicted 3/3 conversions from SCD to MCI (against 1/3 with EEG features). Given the small number of conversions, multicenter studies over longer timescales are required to statistically assess whether our approach is better than the standard one in this respect.

Another limitation lies in the selection of the regions of interest that exhibit impairment. While our work focuses on predicting structural changes linked to AD in the absence of direct structural data, we had to draw from existing literature[20] to determine the regions of interest, referring to the well-known Braak stages[39] (see Methods). This implies that our findings might be influenced by the choice of the impaired regions. To address this, we explored various combinations of impaired regions (based on Aβ and tau Braak stages, their combination, intersection, or considering solely the hippocampus), revealing Aβ Braak stages as the optimal choice; these changes did not qualitatively affect the results (data not shown). Other studies may encompass analyses of regional oscillations, for example, by using high density EEG or source reconstruction software. This can allow to obtain a more precise idea of regional levels of neurodegeneration from EEG recordings.

Third, the aggregation of meso-scale and macro-scale parameters, while facilitating precise model customization and severity assessment, necessitates nuanced assumptions. Specifically, the proportionality between neuroplastic adaptations (represented in the model as increased short-range structural connectivity C_{weight} in impaired regions) and white matter degradation (represented as a decrease of long-range structural connectivity C_{weight}) could be highly subjective.[35,36] While we experimented with diverse ratios of these quantities to identify the most suitable ratio between short-range increase and long-range decrease for our dataset (finally settling for the 1:1 ratio), the inherent subjectivity of deviation from this aggregated value remains unaddressed in this study.

These highlighted challenges delineate promising avenues for future research. One possible direction involves enhancing model realism by integrating structural data from PET or MRI scans into the pipeline, enabling improved identification of impaired regions and quantification of white matter atrophy and neuroplasticity ratios, which significantly influence the model's structural alterations. Continuation of longitudinal follow-up studies on the enrolled patients, already planned, will assess the strength of the model's predictive capacity. Finally, the model could be validated using EEG recordings during tasks that assess cognitive impairments by adding an extension able to capture the effect of visual stimuli.

Advancing the model's power and versatility could involve co-simulations with software like NEST[59] or ANNarchy,[60] mirroring prior applications in the study of deep brain stimulation effects in Parkinson's disease.[61] These multi-scale simulations can encompass alterations extending from microscopic phenomena such as neuron loss in regions like the hippocampus[62] to the meso- and macroscopic effects discussed in our study.[15]

In conclusion, our investigation proposes an innovative path where computational and quantitative EEG analyses converge, extracting pivotal clinical markers and surpassing traditional approaches. The proposed pipeline not only enables the quantification of disease severity through structural insights inferred with non-invasive methods, but also facilitates the prognosis of disease progression, even in patients in prodromal stages of the disease who lack evident symptomatology. This novel approach lays the groundwork for a more affordable and effective diagnosis of neurodegenerative disorders. It holds potential for further evolution through the inclusion of structural imaging modalities and multiscale co-simulations, paving the way for clinical investigations integrating non-invasive biomarkers with computational frameworks, promising rapid and precise monitoring of neurodegenerative conditions.

ACKNOWLEDGMENTS

We thank Dr. Sara Moccia and Angelo Lasala for precious hints on the classification pipeline. This project is funded by Tuscany Region—Predicting the Evolution of SubjectIvE Cognitive Decline to Alzheimer's Disease With machine learning—PREVIEW CUP.D18D20001300002. THE ("Tuscany Health Ecosystem ") Project funded by the Italian Ministry of University and Research—PNRR—Next Generation EU Projects Project funded under the National Recovery and Resilience Plan (NRRP), Mission 4 Component 2 Investment 1.3—Call for tender No. 341 of 15/03/2022 of Italian Ministry of University and Research funded by the European Union—NextGenerationEU Award Number: Project code PE0000006, Concession Decree No. 1553 of 11/10/2022 adopted by the Italian Ministry of University and Research, CUP D93C22000930002, "A multiscale integrated approach to the study of the nervous system in health and disease" (MNESYS)

CONFLICT OF INTEREST STATEMENT

The authors have no relevant conflicts of interest to declare. Author disclosures are available in the supporting information.

DATA AVAILABILITY STATEMENT

Raw EEG data are available upon request for research and scientific purposes. All the code used to perform the simulation and analyses hereby discussed is implemented in Python 3.27. The EEG preprocessing was conducted with the *EEGLAB* MATLAB Toolbox. We used the Python packages Scipy to perform the statistical analyses, MNE to compute EEG features, Sklearn for the machine learning pipeline, and The Virtual Brain software (tvb Python library) to build the model and simulate brain activity. Code is available upon request.

CONSENT STATEMENT

We state that every participant enrolled in this study provided informed consent prior to participation.

REFERENCES

1. Mayeux R, Stern Y. Epidemiology of Alzheimer disease. *Cold Spring Harb Perspect Med*. 2012;2:a006239.
2. Alzheimer's Association. 2018 Alzheimer's disease facts and figures. *Alzheimers Dement*. 2018;14:367-429.
3. Jessen F, Amariglio R, Van Boxtel M. A conceptual framework for research on subjective cognitive decline in preclinical Alzheimer's disease. *Alzheimers Dement*. 2014;10:844-852.
4. Albert M, DeKosky S, Dickson D, et al. The diagnosis of mild cognitive impairment due to Alzheimer's disease: recommendations from the National Institute on Aging-Alzheimer's Association workgroups on diagnostic guidelines for Alzheimer's disease. *Alzheimers Dement*. 2011;7:270-279.
5. Johnson K, Fox N, Sperling R, Klunk W. Brain imaging in Alzheimer's disease. *Cold Spring Harb Perspect Med*. 2012;2:a006213.
6. Mosconi L, Tsui W, Herholz K, et al. Multicenter standardized 18F-FDG PET diagnosis of mild cognitive impairment, Alzheimer's disease, and other dementias. *J Nucl Med*. 2008;49:390-398.
7. Olsson B, Lautner R, Andreasson U, et al. CSF and blood biomarkers for the diagnosis of Alzheimer's disease: a systematic review and meta-analysis. *Lancet Neurol*. 2016;15:673-684.
8. McMahon P, Araki S, Sandberg E, Neumann P, Gazelle G. Cost-effectiveness of PET in the diagnosis of Alzheimer disease. *Radiology*. 2003;228:515-522.
9. Horvath A, Szucs A, Csukly G, Sakovics A, Stefanics G, Kamondi A. EEG and ERP biomarkers of Alzheimer's disease: a critical review. *Front Biosci*. 2018;23:183-220.
10. Poil S, De Haan W, Flier W, Mansvelder H, Scheltens P, Linkenkaer-Hansen K. Integrative EEG biomarkers predict progression to Alzheimer's disease at the MCI stage. *Front Aging Neurosci*. 2013;5:58.
11. McBride J, Zhao X, Munro N, et al. Spectral and complexity analysis of scalp EEG characteristics for mild cognitive impairment and early Alzheimer's disease. *Comput Methods Programs Biomed*. 2014;114:153-163.
12. Zhang H, Wang S, Liu B, et al. Resting brain connectivity: changes during the progress of Alzheimer disease. *Radiology*. 2010;256:598-606.
13. Lassi M, Fabbiani C, Mazzeo S, et al. EEG microstates patterns in subjective cognitive decline and mild cognitive impairment: early biomarkers along the Alzheimer's disease continuum? *Neuroimage Clin*. 2023;38:103407.
14. Farina F, Emek-Savaşÿ D, Rueda-Delgado L, et al. A comparison of resting state EEG and structural MRI for classifying Alzheimer's disease and mild cognitive impairment. *Neuroimage*. 2020;215:116795.
15. D'Angelo E, Jirsa V. The quest for multiscale brain modeling. *Trends Neurosci*. 2022;45(10):777-790.
16. Sanz Leon P, Knock S, Woodman M, et al. The Virtual Brain: a simulator of primate brain network dynamics. *Front Neuroinform*. 2013;7:10.

17. Falcon M, Jirsa V, Solodkin A. A new neuroinformatics approach to personalized medicine in neurology: The Virtual Brain. *Curr Opin Neurol*. 2016;29:429.
18. Wang H, Woodman M, Triebkorn P, et al. Delineating epileptogenic networks using brain imaging data and personalized modeling in drug-resistant epilepsy. *Sci Transl Med*. 2023;15:eabp8982.
19. Stefanovski L, Triebkorn P, Spiegler A, et al. Linking molecular pathways and large-scale computational modeling to assess candidate disease mechanisms and pharmacodynamics in Alzheimer's disease. *Front Comput Neurosci*. 2019;13:54.
20. Stefanovski L, Meier J, Pai R, et al. Bridging scales in Alzheimer's disease: biological framework for brain simulation with The Virtual Brain. *Front Neuroinform*. 2021;15:630172.
21. Hipp J, Hawellek D, Corbetta M, Siegel M, Engel A. Large-scale cortical correlation structure of spontaneous oscillatory activity. *Nat Neurosci*. 2012;15:884-890.
22. Broek S, Reinders F, Donderwinkel M, Peters M. Volume conduction effects in EEG and MEG. *Electroencephalogr Clin Neurophysiol*. 1998;106:522-534.
23. Bastos A, Schoffelen J. A tutorial review of functional connectivity analysis methods and their interpretational pitfalls. *Front Syst Neurosci*. 2016;9:175.
24. Bettus G, Ranjeva JP, Wendling F, et al. Interictal functional connectivity of human epileptic networks assessed by intracerebral EEG and BOLD signal fluctuations. *PloS One*. 2011;6(5):e20071.
25. Chu CJ, Tanaka N, Diaz J, et al. EEG functional connectivity is partially predicted by underlying white matter connectivity. *Neuroimage*. 2015;108:23-33.
26. Boschi A, Brofiga M, Massobrio P. Thresholding functional connectivity matrices to recover the topological properties of large-scale neuronal networks. *Front Neurosci*. 2021;15:705103.
27. Rahi P, Mehra R. Analysis of power spectrum estimation using welch method for various window techniques. *Int J Emerg Technol Eng*. 2014;2:106-109.
28. Schmidt M, Kanda P, Basile L, et al. Index of alpha/theta ratio of the electroencephalogram: a new marker for Alzheimer's disease. *Front Aging Neurosci*. 2013;5:60.
29. Hastie T, Friedman JH, Tibshirani R. *The Elements of Statistical Learning: Data Mining, Inference, and Prediction*. Springer; 2009.
30. Hansson O, Batrla R, Brix B, et al. The Alzheimer's Association international guidelines for handling of cerebrospinal fluid for routine clinical measurements of amyloid and tau. *Alzheimers Dement*. 2021;17:1575-1582.
31. Cummings J. The National Institute on Aging—Alzheimer's Association framework on Alzheimer's disease: application to clinical trials. *Alzheimers Dement*. 2019;15:172-178.
32. Jansen B, Rit V. Electroencephalogram and visual evoked potential generation in a mathematical model of coupled cortical columns. *Biol Cybern*. 1995;73:357-366.
33. Sanz-Leon P, Knock S, Spiegler A, Jirsa V. Mathematical framework for large- scale brain network modeling in The Virtual Brain. *Neuroimage*. 2015;111:385-430.
34. Lauterborn J, Scaduto P, Cox C, et al. Increased excitatory to inhibitory synaptic ratio in parietal cortex samples from individuals with Alzheimer's disease. *Nat Commun*. 2021;12:1-15.
35. Agosta F, Pievani M, Sala S, et al. White matter damage in Alzheimer disease and its relationship to gray matter atrophy. *Radiology*. 2011;258:853-863.
36. Teter B, Ashford J. Neuroplasticity in Alzheimer's disease. *J Neurosci Res*. 2002;70:402-437.
37. Gaubert S, Raimondo F, Houot M, et al. EEG evidence of compensatory mechanisms in preclinical Alzheimer's disease. *Brain*. 2019;142:2096-2112.
38. López-Sanz D, Bruña R, Garcés P, et al. Functional connectivity disruption in subjective cognitive decline and mild cognitive impairment: a common pattern of alterations. *Front Aging Neurosci*. 2017;9:109.
39. Braak H, Braak E, Bohl J. Staging of Alzheimer-related cortical destruction. *Eur Neurol*. 1993;33:403-408.
40. Süli E, Mayers DF. *An Introduction to Numerical Analysis*. Cambridge university press; 2003.
41. Li X, Shi Y. A survey on the Randic index. *MATCH Commun Math Comput Chem*. 2008;59:127-156.
42. Phillips D, McGlaughlin A, Ruth D, Jager L, Soldan A, Alzheimer's Disease Neuroimaging Initiative. Graph theoretic analysis of structural connectivity across the spectrum of Alzheimer's disease: the importance of graph creation methods. *Neuroimage Clin*. 2015;7:377-390.
43. Sporns O. *Networks of the Brain*. MIT press; 2016.
44. David O, Cosmelli D, Friston KJ. Evaluation of different measures of functional connectivity using a neural mass model. *Neuroimage*. 2004;21(2):659-673.
45. Wei Yi-C, Kung YC, Huang WY, et al. Functional connectivity dynamics altered of the resting brain in subjective cognitive decline. *Front Aging Neurosci*. 2022;14:817137.
46. Wang R, Wang J, Yu H, Wei X, Yang C, Deng B. Decreased coherence and functional connectivity of electroencephalograph in Alzheimer's disease. *Chaos*. 2014;24:033136.
47. Jelic V, Johansson SE, Almkvist O, et al. Quantitative electroencephalography in mild cognitive impairment: longitudinal changes and possible prediction of Alzheimer's disease. *Neurobiol Aging*. 2000;21(4):533-540.
48. Meghdadi AH, Stevanović Karić M, McConnell M, et al. Resting state EEG biomarkers of cognitive decline associated with Alzheimer's disease and mild cognitive impairment. *PloS One*. 2021;16(2):e0244180.
49. Tóth B, File B, Boha R, et al. EEG network connectivity changes in mild cognitive impairment—Preliminary results. *Int J Psychophysiol*. 2014;92(1):1-7.
50. Alberdi A, Aztiria A, Basarab A. On the early diagnosis of Alzheimer's disease from multimodal signals: a survey. *Artif Intell Med*. 2016;71:1-29.
51. Gouw AA, Alsema AM, Tijms BM, et al. EEG spectral analysis as a putative early prognostic biomarker in nondemented, amyloid positive subjects. *Neurobiol Aging*. 2017;57:133-142.
52. Malek N, Baker MR, Mann C, Greene J. Electroencephalographic markers in dementia. *Acta Neurol Scand*. 2017;135(4):388-393.
53. Triebkorn P, Stefanovski L, Dhindsa K, et al. Brain simulation augments machine-learning—based classification of dementia. *Alzheimers Dement*. 2022;8:e12303.
54. Vecchio F, Miraglia F, Marra C, et al. Human brain networks in cognitive decline: a graph theoretical analysis of cortical connectivity from EEG data. *J Alzheimer's Dis*. 2014;41(1):113-127.
55. Strik WK, Chiaramonti R, Muscas GC, et al. Decreased EEG microstate duration and anteriorization of the brain electrical fields in mild and moderate dementia of the Alzheimer type. *Psychiatry Res Neuroimaging*. 1997;75(3):183-191.
56. Stam CJ, van der Made Y, Pijnenburg YA, Scheltens P. EEG synchronization in mild cognitive impairment and Alzheimer's disease. *Acta Neurol Scand*. 2003;108(2):90-96.
57. Sibilano E, Brunetti A, Buongiorno D, et al. An attention-based deep learning approach for the classification of subjective cognitive decline and mild cognitive impairment using resting-state EEG. *J Neural Eng*. 2023;20(1):016048.
58. van Nifterick AM, Gouw AA, van Kesteren RE, et al. A multiscale brain network model links Alzheimer's disease-mediated neuronal hyperactivity to large-scale oscillatory slowing. *Alz Res Therapy*. 2022;14:101. doi:10.1186/s13195-022-01041-4

59. Gewaltig M, Diesmann M. Nest (neural simulation tool). *Scholarpedia*. 2007;2:1430.
60. Vitay J, Dinkelbach H, Hamker F. ANNarchy: a code generation approach to neural simulations on parallel hardware. *Front Neuroinform*. 2015;9:19.
61. Meier J, Perdikis D, Blickensdörfer A, et al. Virtual deep brain stimulation: multiscale co-simulation of a spiking basal ganglia model and a whole-brain mean-field model with The Virtual Brain. *Exp Neurol*. 2022;354:114111.
62. Barnes J, Bartlett J, Pol L, et al. A meta-analysis of hippocampal atrophy rates in Alzheimer's disease. *Neurobiol Aging*. 2009;30:1711-1723.

SUPPORTING INFORMATION

Additional supporting information can be found online in the Supporting Information section at the end of this article.

How to cite this article: Amato LG, Vergani AA, Lassi M, et al. Personalized modeling of Alzheimer's disease progression estimates neurodegeneration severity from EEG recordings. *Alzheimer's Dement*. 2024;16:e12526.
https://doi.org/10.1002/dad2.12526